Thin Solid Films 558 (2014) 455–461

Contents lists available at ScienceDirect

Thin Solid Films

journal homepage: www.elsevier.com/locate/tsf

Molecular dynamics simulation of heat conduction in Si nano-films induced by ultrafast laser heating

Yu Zou [a,b], Jun Cai [a], Xiulan Huai [a,*], Fang Xin [a], Zhixiong Guo [c,*]

[a] Institute of Engineering Thermophysics, Chinese Academy of Sciences, 11 Beisihuanxi Road, Beijing 100190, People's Republic of China
[b] Beijing Institute of Petrochemical Technology, 19 Qingyuanbei Road, Beijing 102617, People's Republic of China
[c] Department of Mechanical and Aerospace Engineering, Rutgers, The State University of New Jersey, 98 Brett Road, Piscataway, NJ 08854, USA

ARTICLE INFO

Article history:
Received 8 August 2013
Received in revised form 21 February 2014
Accepted 21 February 2014
Available online 28 February 2014

Keywords:
Molecular dynamics simulation
Heat conduction
Silicon
Thin films
Ultrafast laser heating
Temperature
Pressure
Strain

ABSTRACT

Molecular dynamics simulations are carried out to study the thermal and mechanical phenomena of heat conduction induced by ultrafast laser heating of nanoscale Si films. A distribution of internal heat source obeying Beer–Lambda law is applied to model the laser energy deposition in the film and to calculate the induced temperature and stress distributions. Thermal waves are observed from the local temperature temporal variations and spatial distributions. The developments of averaged static pressure and local displacement in the film show a consistent periodicity. The time evolutions of both the local pressure and net heat flux fluctuate strongly, but show similar trends between these two local physical quantities, demonstrating a close relationship between the stress and the net heat flow.

1. Introduction

Ultrafast lasers have been widely applied to thin film surface modifications and diagnostics related to medical science and engineering [1,2], micro/nano machining [3,4], high-density information storage [5], to name a few. Understanding basic thermodynamic phenomenon of interaction between ultrafast lasers and materials is critical. The mechanism of energy conversion and transport process is one important problem in basic research of many fields like energy, information technology, material processing, micro/nano fabrication, etc. It manifests the interaction of energetic-particles with material at the nano/pico level, whereas the time and space scales of these interactions are in the range of femtosecond–picosecond and nanometer, respectively. Ultrafast laser pump-probe technology provides an avenue to investigate and observe such interactions [6–8].

An early study on micro heat transport induced by ultrafast laser exciting in metal films was carried out in 1980s [6]. The ensuing series of meticulous and in-depth work last until today, mainly focusing on metal materials [3,6–13] with some extension to semiconductors [14], dielectric materials [1,2], and polymers [4]. Some theoretical models on micro/nano non-equilibrium heat transport include heat wave Cattaneo and Vernotte (CV) model [15] that is also known as non-Fourier phenomenon, Anisimov's [16] semi-classical two-temperature model (TTM) that describes a non-equilibrium state between electrons and the lattice, Tzou's [17] dual-phase-lagging model, and models based on plasma formation rate equation [14,18]. Specially, TTM model could effectively describe heat transport in metal films under ultrafast laser irradiation. With the mutual verification and promotion of experiments and theories, research on micro/nano non-equilibrium heat transport in metals has become quite mature today. Nevertheless, theoretical research on nanoscale heat transport in semiconductors and superlattices, a large class of materials, is still scarce.

In microelectronics, nanophotonics, and general IT industries, semiconductors are used more widely than metals. It makes the research on the mechanism of micro/nano heat transport in semiconductor materials bear practical significance. With the improvement of integration of micro/nano electronic and photo-electronic devices, heat problems in semiconductor chips like temperature fluctuation and heat dissipation begin to play a bottleneck role in the development of modern chips.

In the analysis of ultrafast laser induced heat conduction, the triggered pressure waves develop rapidly at the nanometer space scale and in an extremely short pulse heating time. This brings many obstacles for examining thermo-mechanical waves using the above-mentioned theoretical models [19,20]. Under such extreme conditions, continuum body hypothesis is questionable for dealing with heat transfer and thermo-mechanical coupling. Use of molecular dynamics (MD) simulation of atomic or molecular motions plays an important role in

* Corresponding authors.
E-mail addresses: hxl@mail.etp.ac.cn (X. Huai), guo@jove.rutgers.edu (Z. Guo).

http://dx.doi.org/10.1016/j.tsf.2014.02.075
0040-6090/

revealing the heat effects during ultrafast laser-material interaction and the mechanism of internal deformation. Via MD simulation, Wang [21] investigated ps laser copper interaction and Shiomi and Maruyama [22] studied heat conduction in a single-walled carbon nanotube by applying a local sub-ps heat pulse.

In this treatise, MD simulation is performed to study the thermal and mechanical phenomena in Si semiconductor nano-films heated by an ultrafast laser pulse in the fs–ps time scale. Calculations are conducted to obtain temperature, stress and strain distributions, and to observe generation and propagation of stress and net heat waves at the fs–ps time scales. The temperature fluctuation is examined as a result of coupling between the heat transfer quantity and the local stress.

2. Model description

In the present MD simulation, Si crystal atoms along the laser-heating path are placed inside an analog box of one absorption length [19]. We considered five different absorption lengths of 32.3 nm, 40.4 nm, 48.4 nm, 60.5 nm and 75.6 nm, respectively. The reason is twofold: 1) solid thin films with the sizes of several tens of nanometers were frequently employed to investigate heat transport in nanoscale systems and many researchers considered the transition of heat transport mode in Si thin film from ballistic to diffusive regime within this range [19–22]; and 2) light absorption in Si is wavelength-dependent. The absorption length of bulk Si at 300 K varies from 9.6 nm to 105 nm in a wavelength range 350–400 nm and the reflectance at this range is 50–55% against normally incident irradiation (http://pveducation.org/pvcdrom/materials/optical-properties-of-silicon). To reduce statistical errors in compromising with computation power, all the present simulations use the same number of molecules, namely 288,000 Si atoms.

The common force fields suitable for Si crystals include embedded-atom method potential, modified embedded-atom method potential, Tersoff potential, and three-body Stillinger–Weber (SW) potential. In the present simulation, SW potential is selected as the interaction potential between Si atoms, since it can better embody multi-body potential interaction, ensuring calculation precision and avoiding complex calculation of Tersoff potential to enable more atoms to be engaged in the simulation.

In SW potential, the energy E of an atomic system can be expressed as [23]:

$$\begin{aligned} E &= \sum_i \sum_{j>i} \Phi_2\left(r_{ij}\right) + \sum_i \sum_{j\neq i} \sum_{k>j} \Phi_3\left(r_{ij}, r_{ik}, \theta_{ijk}\right), \\ \text{where } \Phi_2\left(r_{ij}\right) &= A_{ij}\varepsilon_{ij}\left[B_{ij}\left(\frac{\sigma_{ij}}{r_{ij}}\right)^{p_{ij}} - \left(\frac{\sigma_{ij}}{r_{ij}}\right)^{q_{ij}}\right] \exp\left(\frac{\sigma_{ij}}{r_{ij}-\alpha_{ij}\sigma_{ij}}\right), \\ \Phi_3\left(r_{ij}, r_{ik}, \theta_{ijk}\right) &= \lambda_{ijk}\varepsilon_{ijk}\left[\cos\theta_{ijk} - \cos\theta_{0ijk}\right]^2 \exp\left(\frac{\gamma_{ij}\sigma_{ij}}{r_{ij}-\alpha_{ij}\sigma_{ij}}\right) \exp\left(\frac{\gamma_{ik}\sigma_{ik}}{r_{ik}-\alpha_{ik}\sigma_{ik}}\right). \end{aligned} \tag{1}$$

In this formula, Φ_2 is two-body potential term; Φ_3 represents three-body potential term; A, B, p and q describe two-body potential interaction; λ and γ are used to describe three-body potential interaction; ε, σ and α are used to describe interaction of both two-body potential and three-body potential; subscripts i, j, and k are atom indices; θ_{ijk} is the angle between $\mathbf{r}_j$ and $\mathbf{r}_k$ subtended at vertex i.

A Gaussian temporal distribution is assumed for the laser pulse whose intensity is [10]:

$$I(t) = I_0 \exp\left[-4\ln 2\left(\frac{t}{t_p}\right)^2\right] \tag{2}$$

where t_p is the pulse width. In all the present simulations, t_p is assumed to be 10 ps. Since a radiation wave will pass through a nano-film in less than 1 ps, the effect of radiation propagation with speed of light [1] is negligible. In the spatial domain, the laser intensity is assumed to be evenly distributed on the irradiation nano-surface with energy per area of a single pulse, Q. Through integration over two infinite time limits one can obtain:

$$I_0 = 0.94\frac{Q}{t_p} \tag{3}$$

If we neglect the scattering of light in Si thin films and accordingly to Beer–Lambda law, the internal heat source converted from laser energy deposition in the Si film is expressed as:

$$S(x,t) = (1-R)\frac{I_0}{\delta}\exp\left[-\frac{x}{\delta} - 4\ln 2\left(\frac{t}{t_p}\right)^2\right] \tag{4}$$

where R is the light reflectance at the film surface, δ is the Si absorption length against the incident laser, and x is the laser penetration location along the film depth direction.

In the present MD simulations, the reflectance is approximated as 50% in the wavelength range 350–400 nm and the internal heat source joins the simulation system in the form of kinetic energy. The Si film model consists of two zones, as shown in Fig. 1. Zone 1, having the length of one absorption depth δ, is of primary interest. Through Eq. (4), the energy deposited into each Si atom can be calculated and determined by x-location of an atom. Considering the random distribution and the principle of uncertainty, the specification of an atom location is only of statistical meaning. Thus, we further divide Zone 1 into 10 equal-thickness sub-zones of same atom number and distribute the deposited energy in a sub-zone to all the atoms inside the sub-zone. The addition of heat is done through speed calibration. The heat is controlled such that no phase change in the film occurs. The laser incident end of the Si crystal film is treated as a free boundary. Zone 2 is a Langevin hot bath to transfer the heat generated by the internal heat source in Zone 1 out of the system through Langevin damping force. The temperature at the exit end of Zone 2 maintains constant, assembling a semi-infinite heat conduction model.

Fig. 2(a) is a diagram of Si crystal cell, in which the side length is 0.543070 nm. The laser incident surface is $fcc(1,1,1)$ surface, as shown in Fig. 2(b), which is built with Si crystal cells. The surface side lengths are 0.384008 nm and 0.665122 nm, respectively.

The present MD simulation consists of an equilibrium stage and a non-equilibrium stage. In the stage of equilibrium simulation, the film is assumed a uniform equilibrium temperature at 300 K initially. The Si volume is determined according to the lattice constant of Si crystal. Canonical ensemble simulation is adopted in the equilibrium-stage simulation.

In the stage of non-equilibrium simulation, laser heat is added to atoms through speed calibration. The four side boundaries parallel to the heat flow direction are in periodic boundary condition to eliminate the boundary effect. The time step used in the simulation is 0.1 fs. Newton motion equation is in the format of leap-frog:

$$\begin{aligned} v_i\left(t+\frac{\delta t}{2}\right) &= v_i\left(t-\frac{\delta t}{2}\right) + \delta t\frac{F_i(t)}{m_i} \\ r_i(t+\Delta t) &= r_i(t) + \delta t\cdot v_i\left(t+\frac{\delta t}{2}\right) \end{aligned} \tag{5}$$

where F is the force, m is the atom mass, r is the displacement of atom, and v is the atom velocity.

The temperature statistical equation in the non-equilibrium stage can be derived from the statistical theory, in which the total kinetic energy, E, is:

$$E = N\bar{\varepsilon} = \frac{3}{2}Nk_BT \tag{6}$$

in which $\bar{\varepsilon}$ is the average kinetic energy of a single Si atom with 3 degrees of freedom, k_B is the Boltzmann constant, and N is the number

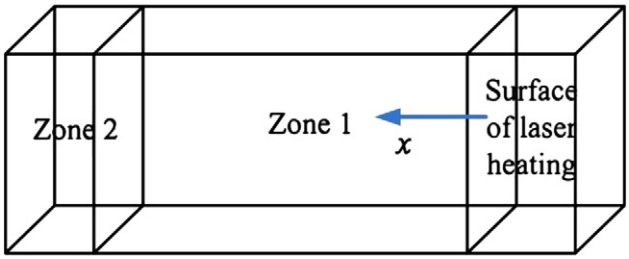

Fig. 1. Schematic diagram of the simulation model in the Si nano-film.

of total Si atoms in a sub-zone. On the other side, the total kinetic energy can also be calculated by

$$E = \sum_{i=1}^{N} \frac{1}{2} m_i v_i^2 \tag{7}$$

Combining Eqs. (6) and (7), it follows that

$$T = \frac{1}{3Nk_b} \left(\sum_{i=1}^{N} m_i v_i^2 \right) \tag{8}$$

The strain corresponds to the displacement absolute value in the centroid of a control volume along the heat flux relative to the interactive force on the boundary of the control volume. In the stage of non-equilibrium simulation, the statistical equation of static pressure in a control volume is:

$$P = \frac{N}{V} k_B T - \frac{1}{3V} \left(\sum_i \sum_{j>i} \frac{\partial \phi}{\partial r_{ij}} \cdot r_{ij} \right) \tag{9}$$

where V is the volume, and ϕ is the potential of the pair atoms. The sum of all interactive forces of atomic clusters within each control volume can be recorded as interactive forces among grids [24]. The pressure tensor of atom i can be recorded as [25]:

$$\begin{aligned} S_{ab} = -\Bigg[& m v_a v_b + \frac{1}{2} \sum_{n=1}^{N_p} (r_{1a} F_{1b} + r_{2a} F_{2b}) + \frac{1}{2} \sum_{n=1}^{N_b} (r_{1a} F_{1b} + r_{2a} F_{2b}) \\ & + \frac{1}{3} \sum_{n=1}^{N_a} (r_{1a} F_{1b} + r_{2a} F_{2b} + r_{3a} F_{3b}) + \frac{1}{4} \sum_{n=1}^{N_d} (r_{1a} F_{1b} + r_{2a} F_{2b} \\ & + r_{3a} F_{3b} + r_{4a} F_{4b}) + \frac{1}{4} \sum_{n=1}^{N_i} (r_{1a} F_{1b} + r_{2a} F_{2b} + r_{3a} F_{3b} + r_{4a} F_{4b}) \\ & + \sum_{n=1}^{N_f} r_{ia} F_{ib} \Bigg] \end{aligned} \tag{10}$$

In formula (10), the first term in the right-hand side is the kinetic energy contribution term. The second term is the two-body potential contribution term, in which the sum term aims at all n atoms in the N_p neighbor list; r_1 and r_2 are the positions of two atoms in the two-body potential; F_1 and F_2 are the interactive forces between two atoms in the two-body potential. The third term is the bonding interaction contribution term. The fourth term is the bond angle interaction contribution term. The fifth term is the dihedral interaction contribution term. The sixth term is the obtuse dihedral interaction term. The seventh term is the interaction term caused by the inner heat source. Three different values are taken for a and b to generate 9 components. To obtain the temperature and stress distributions along the heat flow direction, the 10 equal-thickness sub-zones in Zone 1 contain same number of atoms. The components in the direction of heat flow are summed to obtain the static pressure for each sub-zone.

The statistical Green–Kubo method [26] for heat conductivity can be employed to calculate the net heat flux, J, in the x-direction through a grid:

$$J = \frac{1}{V} \sum_i \left[\frac{1}{2} \left(m_i v_i^2 + \sum_{j \neq i} \Phi_{ij} \right) v_i + \frac{1}{2} \sum_{i<j} f_{ij} \cdot \left(v_i + v_j \right) x_{ij} \right] \tag{11}$$

where f is the force between a pair of atoms.

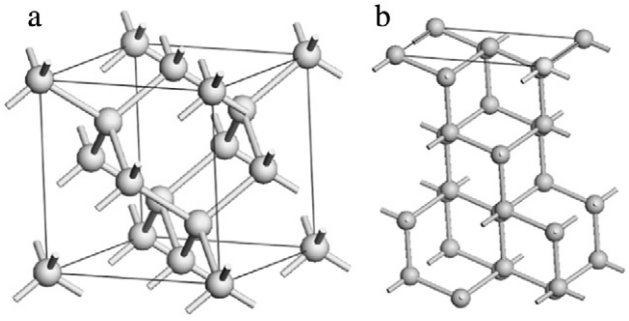

Fig. 2. (a) Diagram of Si crystal cell; and (b) diagram of Si lattice fcc (1,1,1) surface.

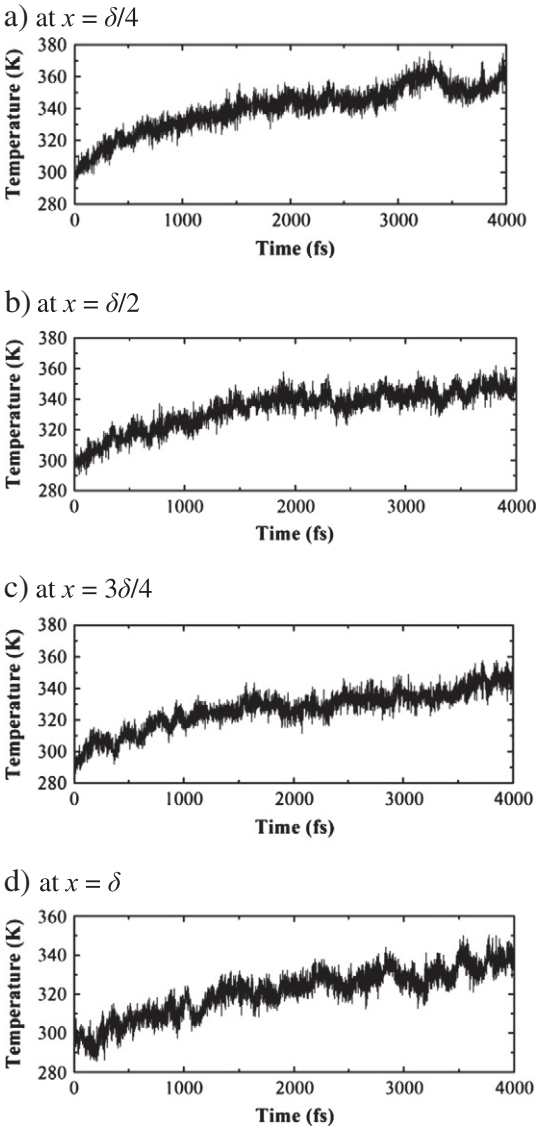

Fig. 3. Time development of local temperature at various depths: (a) at $x = \delta/4$; (b) at $x = \delta/2$; (c) at $x = 3\delta/4$; and (d) at $x = \delta$.

3. Results and discussion

Fig. 3(a–d) shows the time evolution of temperature at four different locations along the heat-flow direction for the 32.3-nm thick film. It displays the existence of heat waves, though the calculated temperature curve concussion may lessen the heat wave appearance. It is also seen that, the change magnitude of temperature with time is different at different depths. The temperature rises faster as the location moves closer to the laser incident surface. Same phenomena were also observed for films of other thicknesses studied. It is well known that heat transfer in nano-structures is significantly different from that in macro-systems. When Knudsen number is above a certain value, the transport mode will change from the diffusive transport to wave propagation (ballistic model), and the usual Fourier law is not appropriate any more [27,28]. In order to make the Fourier law cover the nanoscale, Jou et al. [29] proposed a phenomenological approach of heat transfer in nano-systems within the framework of extended irreversible thermodynamics. In their method, a generalized effective thermal conductivity model was proposed as a function of temperature, mean free path and length of the system. The resultant generalized transport equation will yield a finite speed of propagation.

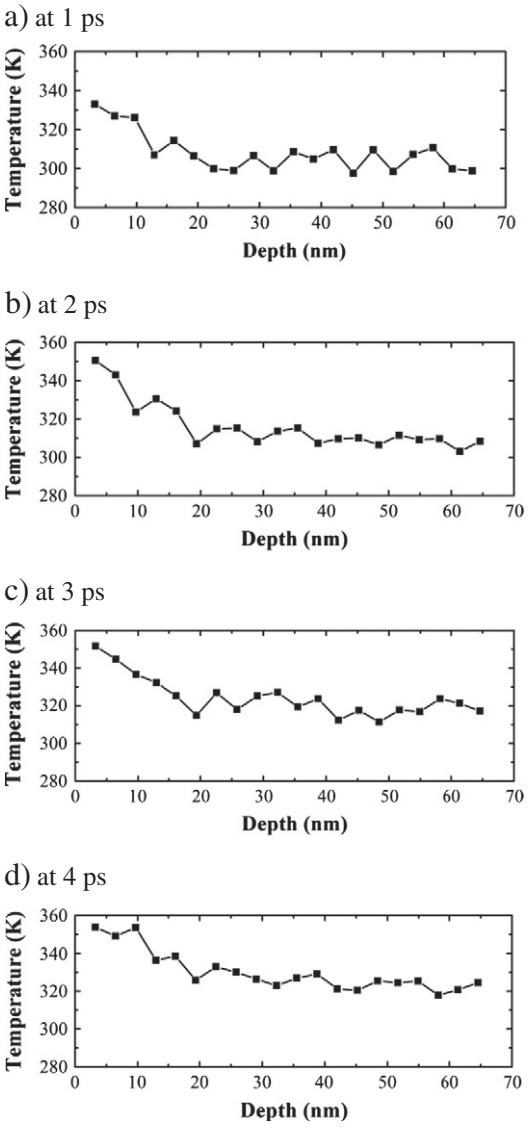

Fig. 4. Temperature distributions along the Si film at various time instants: (a) at 1 ps; (b) at 2 ps; (c) at 3 ps; and (d) at 4 ps.

Fig. 4(a–d) shows the spatial profiles of temperature along the film depth at four different time instants for the film of $\delta = 65$ nm. The periodic variation of temperature indicates the existence of non-Fourier heat waves due to the domination of the ballistic model in the Si nano-film. The peaks in the figures capture the situation of an energy wave traveling in the crystal. The energy wave continues to decline in the process of propagation. Shiomi and Maruyama [22] named this kind of energy wave as the fast Fourier heat wave. Because the time step used in the present MD simulation is extremely fine (0.1 fs) and the overall time scale of the calculation is only 4 ps, it's easy to capture the heat waves. From the present MD data, the heat wave in the Si film travels along the heat flow direction at a speed of 840 m/s, which qualitatively agrees with the speed of propagation calculated by the generalized transport equation [29]. This implies that the present MD method is useful to discern on the validity of thermodynamic formulations of heat transport in nano-systems. From the present results, it is also noted that the propagation speed of heat wave in the Si nanofilm is slower than that of fast Fourier heat wave travelling along a Platinum film, reported as 3400 m/s in the literature [30].

In nano-systems, heat transport is of the ballistic transport regime, not of the diffusive regime. In such regime, the system changes instantaneously and is far from equilibrium. This is also true for heating via ultrafast lasers in ultrashort time because there is no enough time for heat in the thin film to relax. It is noticed that Alvarez and Jou [31] recently proposed a distribution function to elucidate the statistics and fluctuations in ballistic non-equilibrium systems. In MD simulations, the non-equilibrium temperature can be directly obtained via equaling the classic and statistical expressions for kinetic energy as derived in Eq. (8).

Fig. 5 shows the time development of the static pressure averaged over the whole Si film of 48.4nm in thickness. It is seen that the film static pressure changes periodically with time when laser energy is deposited in the Si film. For other Si film thicknesses, this periodic phenomenon also exists. The time period of variation in Fig. 5 is measured to be 730 fs.

Fig. 6(a–e) shows the detailed variation of local static pressure (stress) at five representative locations for the 75.9 nm-thick Si film. It is seen that fluctuation in the local pressure profiles is very strong because of the statistics in the MD simulation as well as the local temperature fluctuation. To minimize such fluctuations, a waveform function regression is made, and the dotted curves in the figures are plotted from the regression fittings. Nevertheless, the regression curves may not fit well because the fluctuations are too strong; and the time period of the fitted waveform functions varies with location and is quite different from the value obtained in Fig. 5 for the averaged pressure variation. The strong uncertainty in the local stress data makes it difficult to find the oscillation period accurately.

Fig. 7(a–d) shows the development of centroid displacement (strain) at four different locations at the Si film of 75.9 nm in thickness. The waveform function regression fitting curves (dotted) are also plotted in the figures. For the displacement, its statistical fluctuations are much lessened as compared with the local pressure data shown in Fig. 6. The fitted curves can generally match with the MD simulated

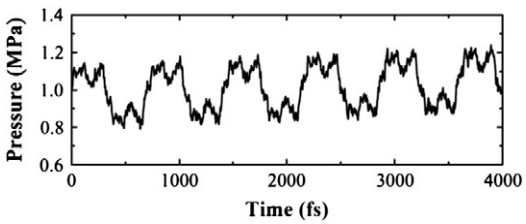

Fig. 5. Time development of the averaged static pressure in the Si film.

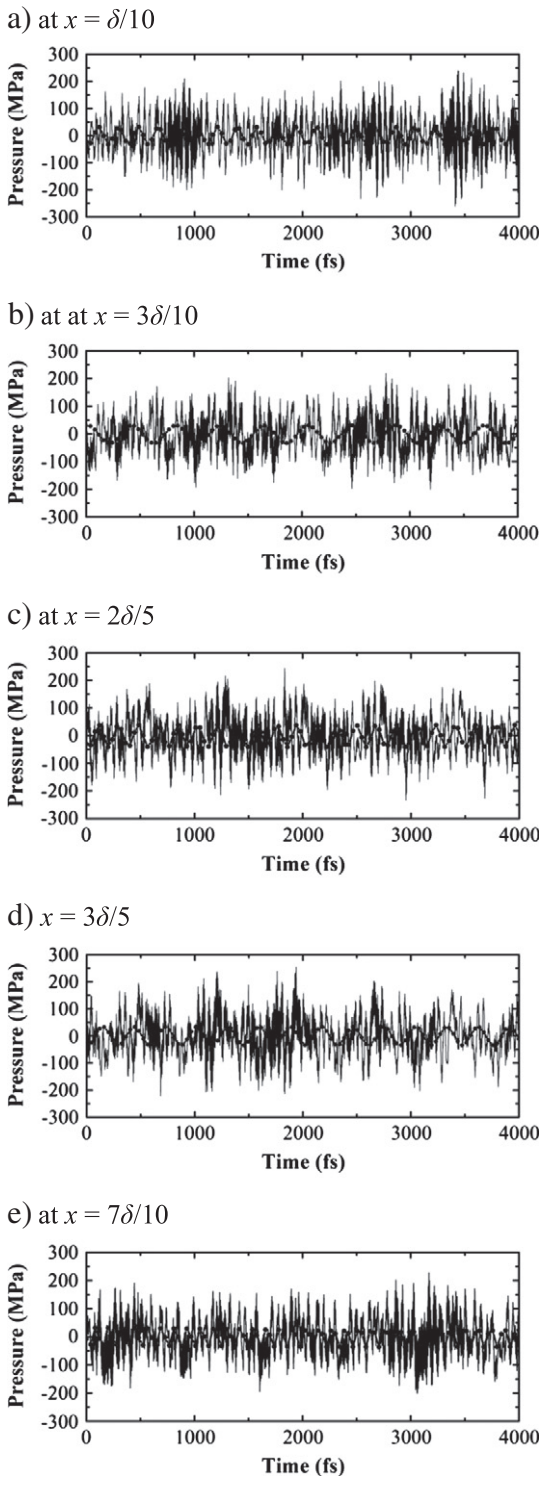

Fig. 6. Time development of local pressure at various depths: (a) at $x = \delta/10$; (b) at $x = 3\delta/10$; (c) at $x = 2\delta/5$; (d) at $x = 3\delta/5$; and (e) at $x = 7\delta/10$.

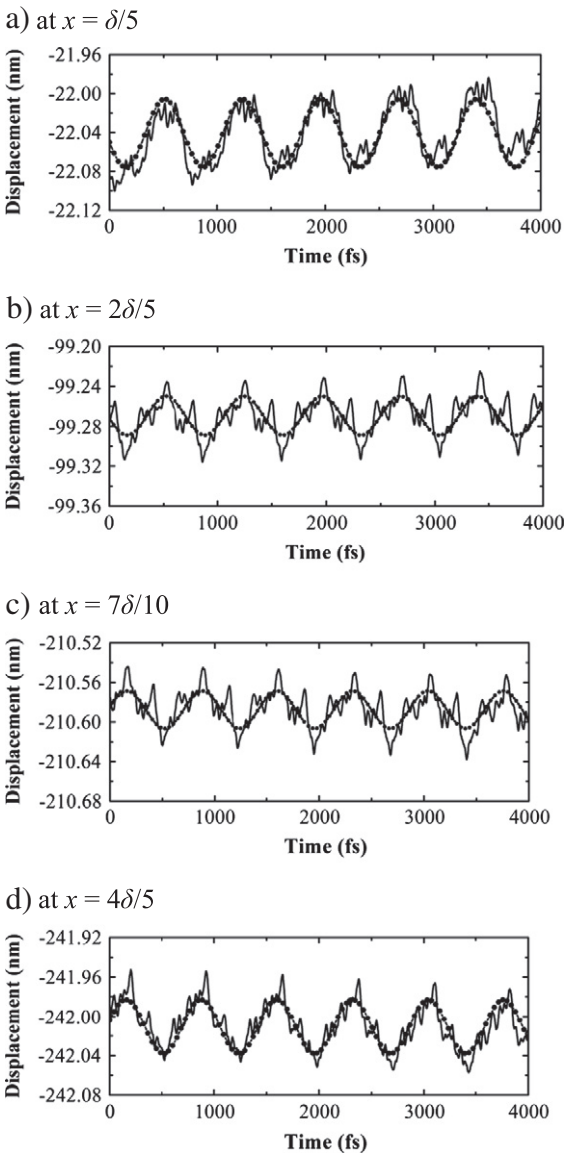

Fig. 7. Time development of centroid displacement at various depths: (a) at $x = \delta/5$; (b) at $x = 2\delta/5$; (c) at $x = 7\delta/10$; and (d) at $x = 4\delta/5$.

variations. Moreover, the time period of displacement variations is close to the value (730 fs) found in the averaged pressure variation shown in Fig. 5, indicating that the displacement is related to the averaged pressure in the film.

Fig. 8(a–g) shows the time development of net heat flux at various locations in the 75.9nm-thick Si film. The dotted curves are from waveform function regression fitting. The strong fluctuations appear again in the net heat flux figures, though they are not as strong as those for the local pressure variations shown in Fig. 6. However, the variation tendencies with location and the time periods between these two local physical quantities are very similar, suggesting that the transport of heat wave in the film and the local pressure are closely related.

For heat conduction in thin films, Fourier law purely considering the diffusive transport will predict an infinite heat flux when time approaches zero (such as in ultrashort laser pulse period) or when the film thickness is smaller than the mean free path of heat carriers. Moreover, it implies an infinite velocity of heat propagation. Although the CV model [15] can solve this problem, it cannot predict temperature jump at the boundary; and thus, it is valid only for larger length scales. An alternative C–F model associated with both Cattaneo's (C) and Fourier (F) processes includes both diffusive transport and wave propagation. In this model, a non-dimensional factor, F_T, is introduced to evaluate the contribution of diffusive heat transport. It recovers Cattaneo's equation when $F_T = 0$, while the diffusive Fourier law is obtained when $F_T = 1$. With the ultrafast laser heating boundary condition in the present study, heat fluctuations (including temperature and heat flux) are observed, which demonstrates the heat wave propagation with a temperature jump at the boundary.

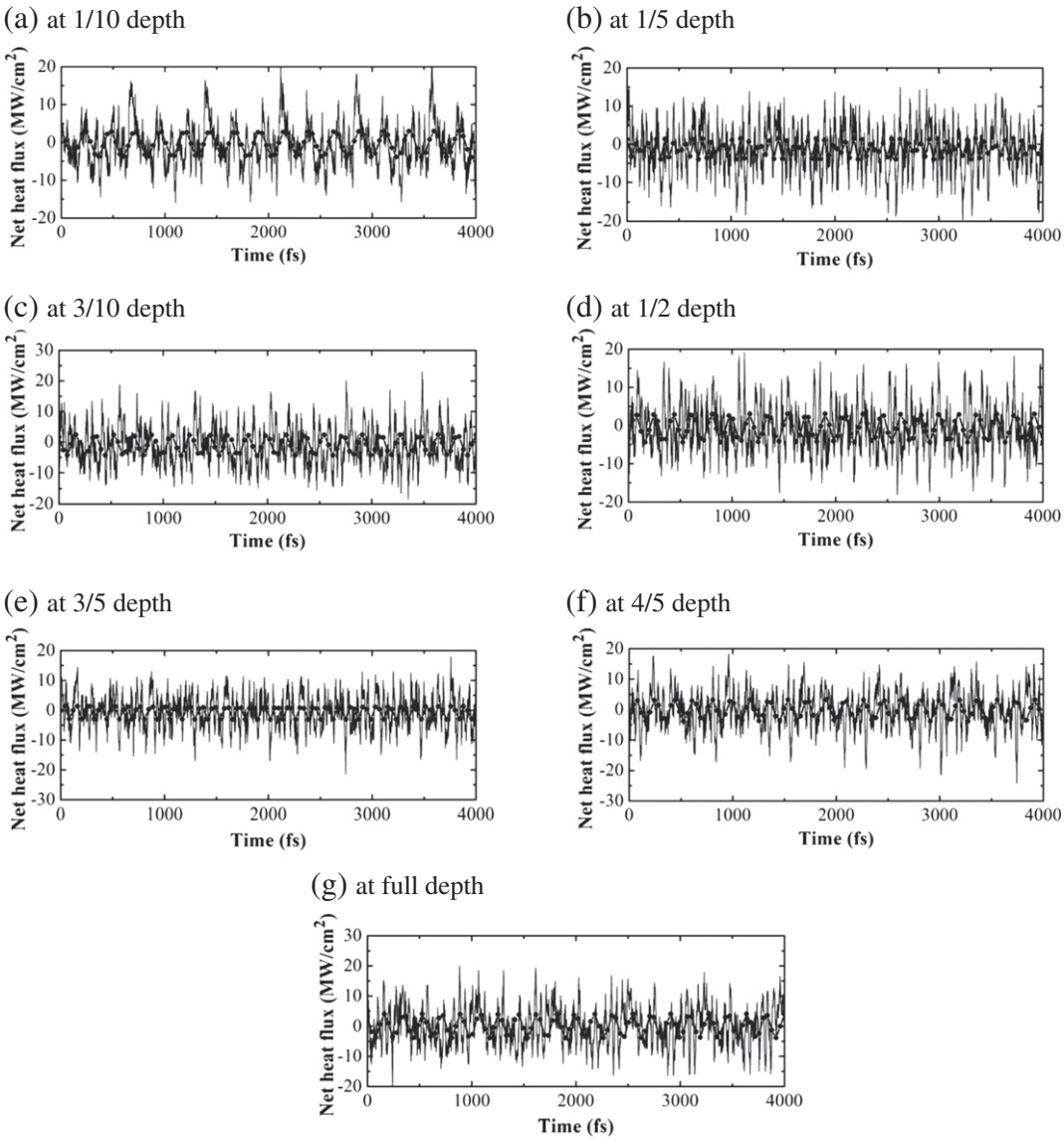

Fig. 8. Time development of net heat flux at various locations: (a) at 1/10 depth; (b) at 1/5 depth; (c) at 3/10 depth; (d) at 1/2 depth; (e) at 3/5 depth; (f) at 4/5 depth; and (g) at full depth.

4. Conclusions

MD simulations are conducted to study the thermal and mechanical phenomena induced by ps laser heating of Si nano-films. The temporal and spatial distributions of temperature, stress, and strain are obtained. During laser heating in the ps time scale, the mean temperature of the film increases monotonically, but the averaged pressure in the nano-film oscillates periodically and increases slowly. The oscillation period of the local strain is consistent with that of the averaged pressure, which is calculated as 730 fs in the Si films. The results also disclose relevance between the local stress and the local net heat, because the developments of these two local physical quantities are similar and both are subjected to extremely strong fluctuations. The wavy variation in temperature distributions demonstrates the existence of heat waves; and the propagation of heat waves is related to the fluctuations of local stress and net heat flux.

Acknowledgments

This research is financially supported by the National Basic Research Program of China (2011CB710705) and the National Natural Science Foundation of China (51076151).

References

[1] Z. Guo, B. Hunter, Heat Transf. Res. 44 (3–4) (2013) 303.
[2] H. Huang, Z. Guo, Lasers Med. Sci. 25 (4) (2010) 517.
[3] A. Chimmaigi, T.Y. Choi, C.P. Grigoropoulos, Appl. Phys. Lett. 82 (8) (2003) 1146.
[4] H. Huang, Z. Guo, J. Micromech. Microeng. 19 (5) (2009) 055007.
[5] J.H. Strickler, W.W. Webb, Opt. Lett. 16 (22) (1991) 1780.
[6] G.L. Eesley, Phys. Rev. Lett. 51 (23) (1983) 2140.
[7] J.G. Fujimoto, J.M. Liu, E.P. Ippen, N. Bloembergen, Phys. Rev. Lett. 53 (19) (1984) 1837.
[8] H.E. Elsayed-Ali, T.B. Norris, M.A. Pessot, G.A. Mourou, Phys. Rev. Lett. 58 (12) (1987) 1212.
[9] H.E. Elsayed-Ali, T. Juhasz, G.O. Smith, W.E. Bron, Phys. Rev. B 43 (5) (1991) 4488.
[10] T.Q. Qiu, C.L. Tien, J. Heat Transf. 115 (4) (1993) 835.
[11] E.G. Gamaly, A.V. Rode, O. Uteza, M. Samoc, B. Luther-Davies, Appl. Surf. Sci. 197–198 (2002) 730.
[12] P.T. Mannion, J. Magee, E. Coyne, G.M. O'Connor, T.J. Glynn, Appl. Surf. Sci. 233 (1–4) (2004) 275.
[13] B.X. Wu, Y.C. Shin, Appl. Surf. Sci. 253 (8) (2007) 4079.
[14] B.X. Wu, Y.C. Shin, Appl. Surf. Sci. 255 (9) (2009) 4996.
[15] D.D. Joseph, L. Preziosi, Rev. Mod. Phys. 61 (1989) 41.
[16] S.I. Anisimov, B.L. Kapeliovich, T.L. Perel'man, Zh. Eksp. Teor. Fiz. 66 (1974) 776.
[17] D.Y. Tzou, J. Heat Transf. 117 (1) (1995) 8.
[18] J. Jiao, Z. Guo, Appl. Surf. Sci. 258 (2012) 6266.
[19] X.W. Wang, X.F. Xu, Int. J. Heat Mass Transf. 46 (1) (2003) 45.
[20] S. Volz, J.B. Saulnier, M. Lallemand, B. Perrin, P. Depondt, M. Mareschal, Phys. Rev. B 54 (1996) 340.
[21] X.W. Wang, J. Heat Transf. 126 (3) (2004) 355.

[22] J. Shiomi, S. Maruyama, Phys. Rev. B 73 (2006) 205420.
[23] F.H. Stillinger, T.A. Weber, Phys. Rev. B 31 (8) (1985) 5262.
[24] B.Y. Cao, Q.G. Zhang, X. Zhang, K. Takahashi, T. Ikuta, W.M. Qiao, M. Fujii, Acta Metall. Sin. 42 (11) (2006) 1207.
[25] M.P. Allen, D.J. Tildesley, Computer Simulation of Liquids, Oxford University Press, Oxford, 1987.
[26] S.H. Lee, D.K. Park, Bull. Korean Chem. Soc. 24 (2) (2003) 178.
[27] D. Jou, M. Criado-Sancho, J. Casas-Vazquez, J. Appl. Phys. 107 (2010) 084302.
[28] F. Vázquez, J.A. del Río, J. Appl. Phys. 112 (2012) 123707.
[29] D. Jou, J. Casas-Vazquez, G. Lebon, M. Grmela, Appl. Math. Lett. 18 (8) (2005) 963.
[30] X.P. Huang, X.L. Huai, Y. Zou, J. Eng. Thermophys. 30 (9) (2008) 1525.
[31] F.X. Alvarez, D. Jou, Physica A 388 (12) (2009) 2367.